Magnetization reversal of a structurally disordered manganite thin film with perpendicular anisotropy

Marcus Liebmann,* Alexander Schwarz, Uwe Kaiser, and Roland Wiesendanger
Institute of Applied Physics, University of Hamburg, Jungiusstrasse 11, D-20355 Hamburg, Germany

Dong-Wook Kim† and Tae-Won Noh
School of Physics & ReCOE, Seoul National University, Seoul 151-742, South Korea
(Received 1 September 2004; published 31 March 2005)

The field-dependent domain structure of a $La_{0.7}Sr_{0.3}MnO_3$ thin film epitaxially grown on a $LaAlO_3$ (001) substrate has been investigated at low temperatures by magnetic force microscopy. Due to the lattice mismatch, the ferromagnetic thin film is structurally disordered and exhibits a stress induced perpendicular easy axis of magnetization and stripe domains at zero field. The magnetization reversal is imaged in a movielike manner along the easy axis major hysteresis loop. Individual Barkhausen jumps are distinguished as either nucleation, growth, or annihilation processes, and analyzed with respect to size, contrast, and position. Nucleation and annihilation occur only in a limited field range just below saturation while growth due to wall propagation dominates the domain formation. The role of disorder in the material in comparison to demagnetization effects is discussed in detail, particularly with respect to the size distribution of nucleation and annihilation as well as growth processes, domain wall pinning, and preferred nucleation sites.

DOI: 10.1103/PhysRevB.71.104431 PACS number(s): 75.60.Jk, 75.60.Ej, 75.70.Ak

I. INTRODUCTION

The magnetization reversal of a ferromagnet is a technologically very important process which is governed by structural as well as magnetic properties of the material. It is characterized by the hysteresis loop, which consists of a series of discrete magnetization jumps, long known as the Barkhausen effect.[1] Conventionally, this effect has been observed by slowly changing the external magnetic field and picking up voltage pulses in an induction coil around the ferromagnetic sample. Each voltage pulse represents a process of magnetization reversal, and the time integral of the voltage is proportional to the change of magnetic flux through the coil. The thorough evaluation of these Barkhausen jumps yielded important information with respect to the critical behavior in the presence of an external field.[2]

Most investigations of the Barkhausen effect have been carried out by this induction technique, which provides only integral information over the whole sample and is difficult to apply to magnetic thin films because of the lower signal level compared to bulk samples. Thus, few direct observations exist.[3,4] In a recent letter, we demonstrated that magnetic force microscopy (MFM) can visualize the domain evolution forming a hysteresis loop out of many Barkhausen jumps.[5] Their size distribution, recorded in a decreasing field, has been analyzed with respect to their scaling behavior and the physical mechanisms behind them. MFM therefore provides a detailed insight into the physical principles governing nonequilibrium magnetization reversal processes, such as nucleation and domain wall propagation, driven by the external magnetic field variation. Imaging the field dependent magnetization permits relating the Barkhausen jumps directly to the micromagnetic configuration. Since force microscopy enables the observation of domains and surface topography of the same area, the quantitative analysis of these reversal processes in real space reveals the interplay between structural and magnetic properties.

In this article, we investigate the magnetization reversal of a ferromagnetic manganese perovskite thin film $La_{0.7}Sr_{0.3}MnO_3$. The domain structure of this sample at zero field after various magnetization histories has been examined recently.[6] Here, we provide a more detailed and complete, i.e., for increasing and decreasing field, analysis of nucleation, annihilation, and domain wall motion processes. In particular, we clarify the relative contributions of structural properties and demagnetization effects.

II. EXPERIMENTAL SETUP

Topography and magnetic force microscopy data are recorded using a home built low-temperature scanning force microscope (Hamburg Design). The setup of this instrument and our MFM measurement procedure are described in more detail elsewhere.[7] The microscope is located inside an ultrahigh vacuum (UHV) bath cryostat at a temperature of 5.2 K. All MFM experiments have been performed at this temperature. To apply a perpendicular magnetic field of up to 5 T, the microscope is surrounded by a superconducting split-coil magnet. The stability of our instrument is such that the relative tip-sample position (in particular the distance) does not change significantly within one day and during ramping the magnet to high fields.

As force sensors, we use commercially available silicon cantilevers with resonance frequencies $f_0 = 183 - 203$ kHz and force constants $c_z = 40 - 57$ N/m. They are prepared *in situ* by argon ion sputtering and evaporation of nominal 5 nm iron on one triangular side face of the tip pyramid as shown in Fig. 1(a). The geometry of tip and sample surface is sketched in Fig. 1(b). Micromagnetic simulations[8] indicate

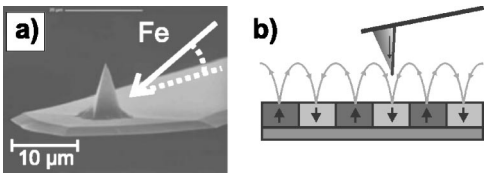

FIG. 1. (a) Scanning electron microscopy image of a typical silicon cantilever showing the direction of the iron evaporation beam. (b) Geometry of the magnetic film with respect to the sample surface. The magnetization directions are indicated by arrows. This configuration responds nearly exclusively to the out-of-plane component of the sample stray field.

that the resulting triangular film develops a strong shape anisotropy, which forces the tip magnetization not only into the film plane but also into the direction of the symmetry axis of the film, pointing towards the tip end. This behavior has been verified by observing the tip magnetization switch in an external field (at typically 30 mT) while imaging a domain structure with a considerably higher coercive field. In this case, the image contrast suddenly inverts, because the magnetization direction of the tip changes by 180° and the formerly attractive interaction becomes repulsive and vice versa. No signs of instability before and after the instantaneous reorientation have been observed. The image contrast on a CoPt multilayer test sample shows that these tips are nearly exclusively sensitive to the out-of-plane component of the sample stray field.

All measurements are performed in the noncontact (NC) regime using the frequency modulation (FM) technique:[9] The cantilever is oscillated by self-excitation with a constant amplitude A_0 at its current resonance frequency f determined by its eigenfrequency f_0 and the tip-sample interaction. The measured quantity is the frequency shift $\Delta f = f - f_0$. For topographic imaging (FM-AFM), the z feedback, which controls the tip-sample distance, is active, and a map of constant Δf is acquired. To record topographic images with a ferromagnetic tip, the sample magnetization is fully saturated at 800 mT to eliminate any magnetostatic crosstalk during data acquisition.

For magnetic force microscopy images (FM-MFM), we apply the plane subtraction mode, i.e., the tilt between tip and sample is compensated by adding appropriate voltages to the z electrode of the scanner, dependent on the xy position. The tip is then scanned in a constant height, $h \approx 20 \cdots 30$ nm, above the sample surface. Since magnetostatic interactions are of long-range nature compared to the oscillation amplitude, the frequency shift is proportional to the force gradient $\Delta f \approx -(f_0/2c_z)(\partial F_z/\partial z)$. Using conventional color coding, bright and dark image regions correspond to attractive and repulsive tip-sample interactions, respectively, and therefore reflect the domain configuration. Topographic crosstalk due to the long-range electrostatic force is eliminated by applying a constant bias voltage U_{bias}, which compensates the average contact potential difference between tip and sample. All images presented in this article show raw data.

III. SAMPLE

The ferromagnetic thin film studied in this work belongs to the class of manganese perovskites, which recently have attracted a lot of attention because of the large variety of coupled magnetic, electronic, and structural effects.[10–13] Following the composition $R_{1-x}A_xMnO_3$, where R is a rare-earth and A is an alkaline-earth element, this class of material exhibits a rich phase diagram with structural, magnetic, and electronic transitions in dependence of composition x and temperature. The most prominent property of some of these compounds is the colossal magnetoresistance effect (CMR), a strong decrease of electrical resistance in an external magnetic field. It has been discovered, among others, in thin films of La-Ba-Mn-O,[14] La-Ca-Mn-O,[15,16] and in our sample material La-Sr-Mn-O (LSMO),[17] which is of particular interest because its Curie temperature lies above room temperature. However, for all materials CMR requires a high magnetic field corresponding to a flux density of several T, which is too large to be useful for applications such as data storage or sensor devices. Therefore, endeavors have been made to explore the low field magnetoresistive behavior (LFMR) of manganites under the influence of extrinsic effects such as grain boundaries, strain, spin-polarized transport in tunneling junctions, and domain-wall magnetoresistance (DWMR).[18] It has been found that LFMR is enhanced if the film exhibits a stress induced magnetic out-of-plane anisotropy[19] and that grain boundaries could provide a significant contribution due to domain wall pinning.[20] Both effects can be investigated by magnetic imaging, analyzing the magnetic configuration in different fields.

A $La_{0.7}Sr_{0.3}MnO_3$ film of 80 nm thickness was deposited on a $LaAlO_3$ (001) substrate by pulsed laser deposition (PLD) at 750 °C and under 10 mTorr oxygen partial pressure. After deposition, the sample has been annealed for 30 min at 600 °C under 500 Torr oxygen atmosphere. This method has already successfully been applied to the growth of other manganese perovskite thin films.[21] Such films grow epitaxially under a compressively stressed *ab* plane and an extended *c* lattice parameter, because the lattice constant of the substrate is 2.4% smaller than that of the film.[22] In order to relax this stress, misfit dislocations are formed in a rectangular pattern along main crystallographic axes.[23] Above a thickness of around 70 nm, the film breaks up into rectangular columns of 20–35 nm in size, separated by amorphous grain boundaries.[24] Magnetically, the distortion of the unit cell leads to an easy axis of magnetization perpendicular to the film plane.

For LSMO on a $LaAlO_3$ (LAO) substrate, the perpendicular anisotropy was confirmed by magnetic force microscopy showing a characteristic maze type stripe pattern.[22] Other investigations focused on the domain pattern in zero field after different field histories,[6,25–27] on the surface morphology,[28] and the field-dependent domain structure in in-plane fields.[25]

After preparation, our sample was transferred under ambient conditions and introduced into the ultrahigh vacuum imaging environment via a load lock. Topographic images (see Sec. VIII) reveal a granular morphology with a rms roughness of 0.4 nm and an average grain size of (32 ± 2) nm, which matches the value obtained from transmission electron microscopy (TEM) investigations on similar samples,[24] but is a little smaller than reported by Desfeux *et al.*, using AFM.[28] However, for AFM these values depend on

the tip radius, because the real surface structure is geometrically convolved with the tip shape. In addition to structural defects, variations of the chemical composition such as strontium segregation have been reported.[29] Note that this does not affect the MFM signal, which originates also from regions below the surface.

Temperature-dependent magnetization data have been acquired using superconducting quantum interference device (SQUID) magnetometry. The Curie temperature was determined from its point of inflection to be $T_C = 325$ K. The saturation polarization at 10 K is $I_S \approx 300$ mT, resulting in a shape anisotropy constant $K_d \approx I_S^2/2\mu_0$ of approximately 36000 J/m^3. For a similarly prepared sample on the same substrate and with nominally identical film thickness, Wu *et al.* determined a substrate induced perpendicular anisotropy of $K_u \approx 20000$ J/m^3.[30] The exchange stiffness A_{ex} can be estimated from T_C by using the Heisenberg model. Assuming that the magnetic interaction is limited to nearest-neighbor Mn sites with the coordination number $z=6$, a spin $S=3/2$, and a lattice parameter $a=389$ pm, the molecular field theory yields $J \approx 3k_B T_C/2zS(S+1) = 3.0 \times 10^{-22}$ J and $A_{ex} \approx JS^2/a = 1.73 \times 10^{-12}$ J/m for the exchange integral and the exchange stiffness, respectively.

IV. FIELD-DEPENDENT DOMAIN STRUCTURE

To study the magnetization reversal, we continuously recorded MFM images while ramping a perpendicular field $\mu_0 H_\perp$ from 0 T to saturation at 600 mT and back to zero field. The stability of our instrument allows this movielike measurement mode without readjusting any imaging parameter during the 22 h of data acquisition time. Thus, every image of this sequence shows the same sample area. The recording of one image took about 8.5 min. Since the ramp rate was varied according to the activity of magnetization reversal processes, each image covers a field range of 5 mT (from 300 up to 500 mT, and 400 down to 200 mT) or 10 mT (others).

Figure 2 shows six images of this movie. Starting from a maze type pattern at remanence, the coercive field is passed at about 75 mT (a), where an equal distribution of dark and bright contrast is observed. With increasing field, antiparallel domains shrink, until just before saturation only domains of circular contrast and opposite polarity remain (b). These circular domains are annihilated at a field above 400 mT, until at 600 mT, the magnetic contrast vanishes because the film is homogeneously magnetized (c). The very few remaining features (such as the most prominent one marked by an arrow) are of topographic origin. They can be used to track the relative tip-sample position throughout the whole measurement. The lateral drift was less than 10 nm, which is approximately the distance of two image pixels. In a decreasing field after saturation, domain formation starts at around 340 mT with the nucleation of few domains which mostly exhibit a circular configuration (d). Below 280 mT, the domains start to become increasingly elongated while new domains still nucleate down to 200 mT. Below this field, only domain growth is observed (e) forming a maze-type domain pattern in remanence (f).

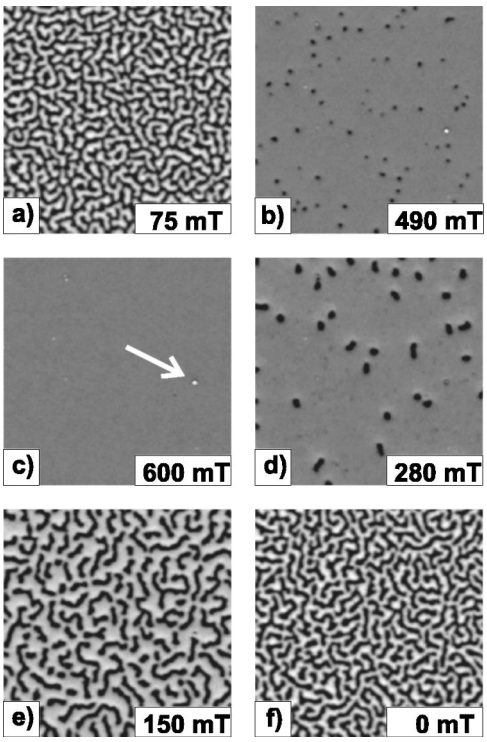

FIG. 2. Magnetization reversal, visualized by MFM. All images cover the same sample area. Bright contrast indicates sites where tip and sample magnetization are parallel. (a) and (b) were recorded in increasing, (d) and (e) in decreasing field. (c) In saturation, a topographic feature, marked by an arrow, can be clearly seen and traced through the whole sequence. Parameters: scan area 4×4 μm^2, $h=24$ nm, $f_0=195$ kHz, $A_0=\pm 5$ nm, $c_z=51$ N/m, scan speed 8 μm/s, $U_{bias}=-100$ mV.

The mean domain width of such an irregular structure can be defined as the ratio of total image area and domain wall length. This value is estimated using a stereological method by drawing arbitrary cross sections of total length l and counting the number n of intersections with domain walls. Then, $w = 2l/\pi n$ represents the domain width matching the common value for parallel aligned stripes (see p. 331 in Ref. 31). In remanence, a mean domain width of $w = 79 \pm 3$ nm is measured, compared to 54 ± 3 nm after thermal demagnetization.[6]

V. QUANTITATIVE ANALYSIS OF THE MFM SEQUENCE

The evolution of domains can be clarified by using the concept of difference images: Since there is no significant drift compared to the domain size during the movie, we can directly subtract two consecutive images in order to show the changes of the MFM contrast. In fact, all images of this movie can be subtracted from each other without further corrections, independent of the difference in their acquisition time. In increasing fields the bright areas grow, because they are magnetized parallel to the external field and the tip magnetization, while in decreasing field the fraction of dark regions increases. Therefore, the difference images exhibit bright contrast in increasing, and dark contrast in decreasing fields.

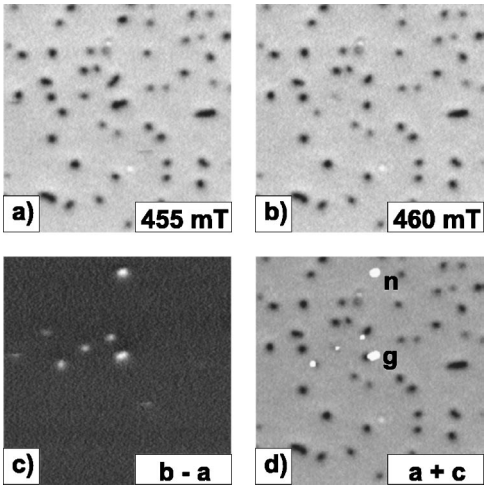

FIG. 3. Identification of annihilation (*n*) and growth (*g*) processes. (a) and (b) show original images in increasing field, (c) the difference image. (d) Changes of the domain structure are highlighted with respect to image (a). For parameters, see Fig. 2.

Figure 3 shows an example of two consecutive images obtained at increasing field (a),(b). The areas of changed magnetization can be found in the difference image (c). In order to distinguish between annihilation and growth, their contours are then plotted into the original image as shown in (d). Contours not connected with dark areas are considered annihilation sites whereas the others are regarded as domain growth due to wall propagation. For decreasing fields, cf., Fig. 2 in Ref. 5, domain nucleation and growth processes can be discriminated in the same way.

In almost all parts of the sequence, the difference images display the changes of sample magnetization as an accumulation of well separated units which can be analyzed individually. These difference images are used to identify and characterize individual magnetization reversal processes, in particular the area, contrast, and the position relative to existing domains.

Imaging ferromagnetic thin films that are basically two dimensional, i.e., the volume is free of magnetic charges, the MFM is sensitive to the magnetic charge density σ at the surface:[31]

$$\Delta f(x,y) = \frac{f_0}{2c_z}\int_S \sigma(x-x',y-y')\frac{\partial H_z}{\partial z}(x',y')dx'\,dy', \quad (1)$$

where H_z denotes the tip stray field. However, for the accurate size measurement of individual processes in the difference images as well as those of isolated domains in a homogeneously magnetized surrounding area, the corresponding apparent areas must be corrected due to the extended stray field of the imaging tip. Since our experiments are performed in the dynamic mode (FM-MFM) with an oscillation amplitude considerably smaller than the decay length of the magnetostatic interaction, the distribution of magnetic surface charges is geometrically convolved with the gradient of the tip stray field. This is equivalent to considering the magnetization of the tip oscillating in the stray field of the sample.

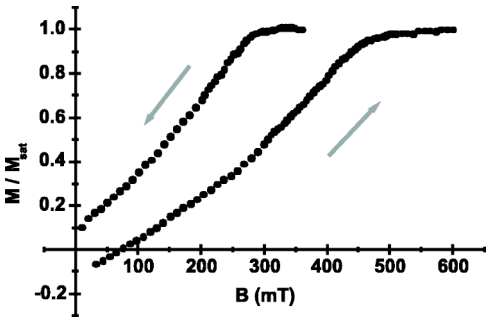

FIG. 4. Hysteresis from the accumulated magnetization changes, computed from all difference images of the sequence recorded over half a major hysteresis loop.

For various scan heights near 25 nm, we have computed the stray field of the magnetic tip coating using micromagnetic simulation.[8] The shape of the corresponding field derivative in the *z* direction can be approximated by evaluating the difference between the stray fields at two scan heights 20 and 30 nm, corresponding to a cantilever oscillation amplitude of ±5 nm. We found that this effect is comparable to a smoothing filter of Gaussian shape with a diameter (FWHM) of 37 nm. As a result, the total apparent area of magnetization changes summed over all difference images is five times larger than the true reversed area calculated from the coercive field image (which is half of the image area). Since the convolution effect is more severe for smaller areas, it is not sufficient to just divide the apparent areas obtained from difference images such as Fig. 3(c) by this single correction factor.

To obtain a better estimate of the true reversed area, A_i, of each individual event, we additionally evaluated the integral of the contrast over the apparent area, a_i, of each event: $K_i = \int_{a_i}(\Delta f - f_{\mathrm{med}})dx\,dy$, where the median contrast, f_{med}, of the image to be analyzed is taken as zero level, that is, to a very good approximation, the mean level of the undisturbed areas. We defined the apparent area as those image pixels where the contrast exceeds the noise level of the neighborhood. K_i, being measured in $\mathrm{Hz}\cdot\mathrm{nm}^2$, is proportional to the underlying magnetic surface charges. The integral of contrast is transformed into a real area using a calibration factor: $A_i = \gamma K_i$, where γ is measured in Hz^{-1}. This factor only depends on the stray field distribution of the tip at the sample surface and can therefore be used for all images of the sequence, for isolated features in difference as well as in original images.

In order to find the value of this calibration factor, the change of integrated contrast in every image is measured, accumulated to form a normalized hysteresis loop (Fig. 4), and finally compared to the actually reversed area. Two calibration points have been used: (a) the saturation magnetization, (b) the average magnetization before and after the reversal of the tip magnetization at 30 mT, computed from original MFM images. At that field, a quasiperiodic structure is observed [Figs. 2(a) and 2(f)], and MFM is able to measure domain widths correctly in this case, because the periodicity of a structure is not altered by the effect of smoothing–only the contrast. However, the change in tip

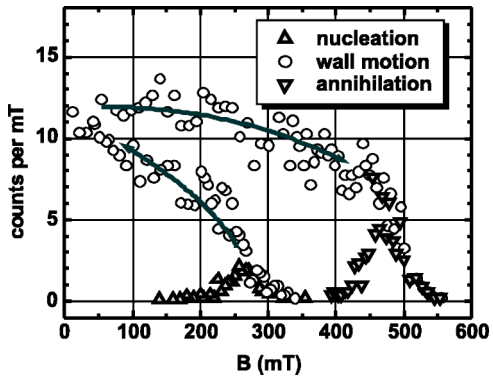

FIG. 5. Number of magnetization reversal processes in increasing and decreasing external field (see arrows), displayed separately for annihilation, nucleation, and domain wall motion. The latter type dominates the evolution of the domain pattern. Significant contributions from annihilation of a domain or nucleation of new domains occur only near saturation.

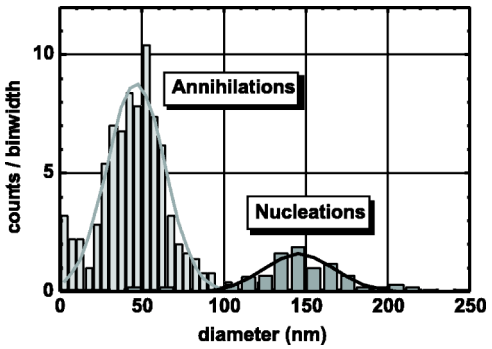

FIG. 6. Size distribution of reversed magnetization areas for annihilation and nucleation. For both, a Gaussian distribution is observed. Mean diameter: 46 nm for annihilation, 146 nm for nucleation.

magnetization from antiparallel to parallel with respect to the external field causes a jump in the percentage of parallel aligned domains, indicating a tip induced contrast deviation of 3.8%. Taking that into account, the mean percentage of parallel aligned domains at 30 mT is 46.6%, that is an area of 8.544 μm^2 to be reversed before saturation. The resulting local hysteresis loop (measured in an area of 16 μm^2) constructed from the evaluation of individual Barkhausen events is well compatible with those obtained from conventionally measured magnetization data determined from the whole macroscopic sample.[32]

VI. NUCLEATION, ANNIHILATION, AND GROWTH

By means of the method depicted in Fig. 3, more than 5000 wall motion and 400 annihilation events could be distinguished on the increasing branch, and about 2000 wall motion and 100 nucleation processes on the decreasing branch of the hysteresis loop from remanence to saturation and back to remanence. In Fig. 5, the number of processes per mT field change is displayed as a function of the external field. The evolution of the domain pattern is dominated by wall motion. Annihilation of the shrinking domains is observed between 400–550 mT, and nucleation of new domains between 340–200 mT. In either case, they occur only near saturation, and the number of wall motion events is always nearly equal or greater than that of any other process.

Figure 6 displays the size distributions of annihilation and nucleation events. In both cases, the distribution can be approximated by a Gaussian profile with a mean diameter of (146 ± 21) nm for nucleations and (46 ± 18) nm for annihilations. The average diameter for domain growth by wall propagation of 41 nm (no significant difference is observed for increasing and decreasing fields) is much smaller than the nucleation diameter, but only slightly smaller than the annihilation diameter. Moreover, growth events do not follow a Gaussian distribution.

Nucleations exhibit a considerably larger diameter than other processes, because they include the formation of a new domain wall which acts as an energy barrier. The creation of a new domain is a thermally activated process which is governed by the presence of surface and volume energy terms. The domain wall energy of a circular domain with radius R is proportional to the wall area $E_w=2\pi\gamma Rt$ (with the film thickness t, and the wall energy per unit area $\gamma=4\sqrt{AK_u}$). The energy E_{ext} of the domain in the external field and the demagnetization energy E_{mag} (for $t\ll R$) are proportional to the magnetic volume: $E_{\mathrm{mag}}=-(2\pi/\mu_0)R^2t|\vec{J}_s|^2$ and $E_{\mathrm{ext}}=(2\pi/\mu_0)R^2t\vec{J}_s\cdot\vec{B}$, where $\vec{J}_s$ denotes the saturation magnetization and $\vec{B}$, the external field.

Whenever such surface and volume energy terms are present, thermodynamics predicts that only those compact fluctuations remain stable, which exceed a certain critical diameter (critical droplet theory).[33] According to this energy balance, we determined a minimum diameter $2R_c=\mu_0\gamma/J_s(J_s-B)$, of 104 nm for the typical nucleation field of 270 mT, where we observed the largest number of nucleations.[5] Considering the simplicity of the model, this result is in reasonable agreement with the observed mean value of 146 nm. In an inhomogeneous material (in our case, the film contains structural disorder), exchange stiffness and anisotropy coefficient, and therefore the energy landscape, will vary locally. Consequently, the critical diameter becomes Gaussian broadened.

For annihilation, the energy balance is different. Here, the wall energy is released and does not serve as an energy barrier. Therefore, annihilation processes can be very small. However, since the observation of an annihilation process requires the previous existence of a stable domain, the size of annihilations reflects the size of the smallest stable domains in this material. For a circular domain in a thin film, the different energy contributions E_i can be converted into generalized pressures acting on the domain wall

$$p_i=-\frac{1}{2\pi Rt}\frac{\partial E_i}{\partial R}, \tag{2}$$

where $2\pi Rt$ denotes the domain wall area. The presence of a domain wall therefore provides an inward pressure p_w comparable to surface tension in a droplet of liquid, being pro-

portional to the curvature of the wall: $p_w \propto 1/R$. The applied external field acts in the same direction, trying to reverse the magnetization into the parallel direction. This pressure does not depend on the domain size or wall curvature but solely on the external field and has the same value for all domains at a given field $p_e \propto |\vec{B}|$.

In order to stabilize the domain wall, these two pressures have to be compensated by the demagnetization effect which tries to minimize the stray field of the magnetic structure by producing equal amounts of parallel and antiparallel magnetized areas and therefore acts as an outward pressure, highly dependent on the domain pattern.

If the external magnetic field rises and the domain radius falls below a certain value (increasing the inward pressure), the domain collapses and is annihilated. Thiele[34] calculated the stability of cylindrical domains in a thin film with uniaxial anisotropy. Given the parameters of our sample (film thickness, saturation magnetization, anisotropy, and exchange stiffness), a minimum diameter of 45 nm can be obtained directly from graphs in the reference, in a very good agreement with the measured mean diameter of (48 ± 16) nm. Note that this calculation does not take into account the pinning of domain walls and local variations of magnetic parameters by structural inhomogeneities which cause a broadening of the size distribution of annihilation processes, as is observed.

The third type of observed events, domain growth processes, is mainly the result of a simple motion of an existing domain wall. For freshly nucleated circular domains in a decreasing field, this mechanism provides a second cause of instability. Whereas the energy of the domain in an external field and, to some extent, the stray field energy depend on R^2, the wall energy is proportional to R. However, it is possible to decrease the overall energy by forming elongated domains (strip out) which reduces the stray field energy at the slight expense of wall energy. This mechanism leads to the final maze type domain pattern at remanence. The stability of a circular domain against elliptical deformations as described has been calculated by Thiele[34] resulting in a maximum diameter of a circular domain of 121 nm for our sample. The observed average diameter of domains just before strip out has been found to be around (130 ± 24) nm.

For an existing domain wall to move, only a minimal energy is required to depin the wall from its present position which might be determined by small inhomogeneities of the film. Therefore, small processes are much more common in this case. The size distribution for areas a_p which are reversed through domain growth is considerably different from nucleation and annihilation processes (Fig. 7). As reported earlier,[5] it follows an inverse power law over three decades and then cuts off exponentially, best described by a fit according to $P(a_p) \propto a_p^{-\tau} e^{-a_p/a_0}$ [increasing field: $\tau = 0.50 \pm 0.04$ and $a_0 = (3295 \pm 189)$ nm^2; decreasing field: $\tau = 0.54 \pm 0.03$ and $a_0 = (6624 \pm 551)$ nm^2]. A purely thermally activated magnetization reversal would result in a simple exponential size dependence. The observed power law dependence is characteristic for systems at criticality. This issue will be examined more detailed in the following section.

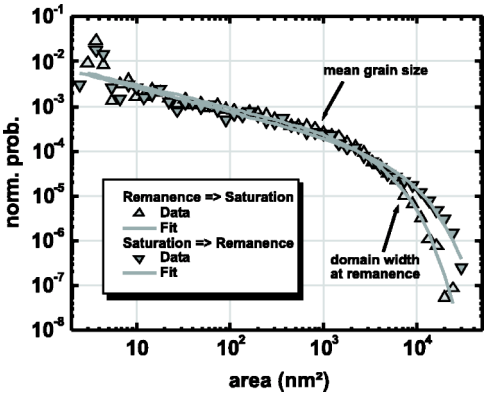

FIG. 7. Size distribution of reversed magnetization areas due to domain wall motion for increasing and decreasing field. It follows an inverse power law over three orders of magnitude. The area of exponential cutoff is different in both cases, indicating a magnetostatic origin, not a structural one. Note that logarithmic binning was chosen.

VII. BARKHAUSEN EFFECT AND CRITICALITY

As can be seen from the difference image in Fig. 3, the field-dependent magnetization evolves through the reversal of discrete units, which cause a sudden change in the magnetic flux within the sample, according to their volume. These steplike changes of magnetization are known as Barkhausen jumps. Conventionally measured through induction experiments, each voltage pulse corresponds to a switching process within the magnetic material, and its time integral is proportional to the change of magnetic flux. We assume that the magnetization of our film does not change in the direction perpendicular to the film plane so that the surface charge, observed by MFM and calculated by means of the above described integration method for the difference images, is proportional to the reversed magnetic moment. The size distributions extracted from induction experiments are then directly comparable to those given here.

Each reversal event (Barkhausen jump) can be regarded as an avalanche of switching spins, caused by a slowly changing magnetic field. These avalanches keep the system in a critical state near the edge of instability. Such a behavior far from equilibrium has recently been discussed under the aspect of self-organized criticality[35] (SOC) and linked to the Barkhausen effect.[2] It is essential that the critical state is not reached by fine tuning of external parameters (as it would be the case in the proximity of phase transitions in equilibrium thermodynamics) but by self-organization. The avalanches show self-similar structures in space as well as in time. Size distributions follow an inverse power law over many orders of magnitude. In experiments[36] as well as in simulations,[37] an exponential cutoff has been observed for large sizes, which has been attributed to a finite size effect, i.e., an avalanche cannot be larger than the investigated system itself. SOC has been applied to a large variety of phenomena, including earthquakes, growing of sand piles, spin density waves, or flux lines in superconductors.[38]

However, it has been argued that SOC is not necessarily needed to obtain such a scaling law.[39] In fact, an inverse

power law distribution followed by an exponential cutoff can be found by modulating the speed of domain wall propagation with statistical fluctuations,[40] e.g., caused by structural disorder. Increasing the intensity of fluctuations would result in a greater critical exponent τ and cutoff area a_0 and therefore enlarge the tendency of criticality. Recently, the predicted critical exponent of $\tau=4/3$ for a single domain wall moving in a disordered two-dimensional system[41] has been experimentally confirmed for a thin film with in plane magnetization.[4] However, this model is not applicable to our situation, because interactions between domain walls were neglected. Furthermore, there are some aspects which contradict criticality by self-organization in our case. To consider a system as governed by SOC, one would expect that critical behavior is observed over a wide range of parameters. On the other hand, a theoretical analysis[42] revealed that criticality is only achieved if the typical length scale of structural disorder ξ is of the same order of magnitude as the magnetic exchange length $l_{\mathrm{ex}} \approx \sqrt{A_{\mathrm{ex}}/K_u}$. Indeed, this condition is fulfilled for our sample, where we can identify ξ with the mean grain size of 32 nm, which is of the same order of magnitude as $l_{\mathrm{ex}} \approx 10$ nm.

The second aspect deals with the physical origin of the exponential cutoff. As mentioned above, in SOC the finite size of the system limits the avalanche size. Obviously, this is not the reason in our case because even the largest observed avalanches are orders of magnitude smaller than the image area, not to mention the sample size. Basically two mechanisms are capable of slowing down and stopping a moving domain wall: pinning at inhomogeneities[39,42] and long-range dipolar interactions.[43] Pinning sites can be provided by grain boundaries which lower the energy of a passing domain wall. To move from one pinning center to the other, the domain wall has to overcome a certain energy barrier, and the probability to do so at an increasing number of barriers decreases exponentially. In fact, the exponential decay of the observed size distribution starts at the same order of magnitude as the mean grain diameter suggests.

The influence of dipolar interactions can be seen from the decrease of the mean size of the reversed areas as the domain pattern approaches the remanent state (Fig. 8). The reversal of large areas becomes more and more unlikely because the domain width of the thermally demagnetized sample (54 nm), which can be considered as an energy minimum, is just around one third of the mean diameter of nucleated domains. Given that size, it is energetically favorable to reduce the average domain width occurring at high fields by adding small areas of magnetization reversal through growth processes at lower fields. Additionally, the hysteresis curve is nearly linear from the initial nucleation towards remanence indicating that the internal field $\vec{B}-\vec{J}(\vec{B})$ is almost constant and very small. As a consequence, large processes are suppressed. The same argument is valid for increasing field, where the mean area remains around 1000 nm^2 in the lower field range (Fig. 8). As long as elongated domains are the most frequent features, the average size remains small. As the magnetization approaches saturation, the change of the internal field becomes more pronounced, and the mean reversal area increases again. The magnetic structure apparently plays an important role for the size of individual processes.

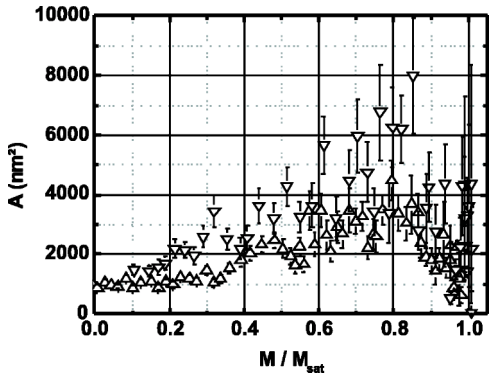

FIG. 8. Average size of growth processes for each image at increasing ($\triangle$) and decreasing ($\triangledown$) field. As the magnetic film approaches remanence, the average size decreases and stays small as long as elongated domains are dominating. The large error at high magnetization is due to the smaller number of observed processes.

Another hint towards the influence of dipolar interaction is given by the comparison of the cutoff area in decreasing and increasing field. While the exponent of the inverse power law remains constant within the experimental error, the cutoff area changes by a factor of 2 (see parameters in Sec. VI), which shows a dependence on the different stages of the magnetic domain evolution. If structural disorder were the origin, both parameters should be unchanged during the whole hysteresis loop. Thus we conclude that the exponential cutoff is most likely determined by dipolar interaction rather than structural disorder.

VIII. CORRELATION WITH TOPOGRAPHY

Since LSMO thin films exhibit a dislocation network and above 70-nm thickness a columnar structure, the question arises whether there is a correlation between the topography and the domain pattern. To address this issue, we chose a sample area without gross topographic features which is thus representative for most parts of the film. On this area, several topographic images were recorded in saturation, each separated by a hysteresis loop. These cycles took several days, however, the lateral drift during that period was less than 10 nm which is considerably smaller than both, the domain width and the mean grain diameter.

Figure 9 displays the contours of MFM images in remanence (a) and during the early stages of nucleation (b) together with the topography of the same area. In (a), no correlation with the topography is visible, e.g., the domain width is larger than the grain size and the domain boundaries do neither follow topographical valleys nor ridges. This impression is supported by a numerical cross correlation. As mentioned before, the topography does not necessarily reflect the internal film structure. Thus, volume pinning sites for domain walls cannot be identified. Furthermore, due to the difference in the contrast formation mechanism, there may be a constant lateral shift between the topography and MFM images.

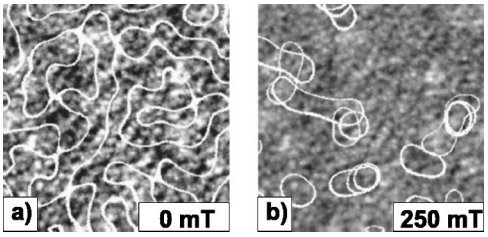

FIG. 9. Correlation of topography and domain structure. (a) Topography including the contour of the domain pattern. The white contour lines correspond to the boundary, i.e., the mean contrast level, between oppositely polarized domains. No obvious correlation is visible. (b) Initial nucleation sites (white contour lines) of three different hysteresis cycles with respect to topography. Evidently, the first few nucleation events occur at nearly identical locations. Image area 1×1 μm^2.

Image (b) contains the contours of the first few nucleated domains, imaged at 250 mT of three different hysteresis loops in the same scan area. Again, there is no correlation with topography, but four areas were centers of initial nucleation in all three loops. Accordingly, there are internal properties of the film which favor nucleations at special sites, not distinguishable by any topographic feature.

Such an influence of subsurface structural inhomogeneities is also supported by a comparison of two zero field images recorded in the same scan area during consecutive hysteresis cycles, as shown in Fig. 10. Representing these images in black and white contrast (see insets), the fraction of white image pixels is $p_a=0.553$ and $p_b=0.544$, respectively. Assuming a purely statistical distribution of black and white regions, the probability that an image pixel did not change its contrast from (a) to (b) is $p_a p_b+(1-p_a)(1-p_b)=0.505$. The histogram (c) of the difference image (b)-(a), however, indicates that a considerably higher fraction did not change its contrast. A value of 0.673 was computed from a three peak Gaussian fit to the data, representing a change from black to white, white to black, and no change, respectively. As suggested by the existence of preferred nucleation sites, the domain pattern is not completely random but in part determined by internal inhomogeneities of the film.

IX. CONCLUSIONS

A detailed magnetic force microscopy study of an epitaxially grown $La_{0.7}Sr_{0.3}MnO_3$ thin film on a $LaAlO_3$ (001) substrate is presented, which exhibits a perpendicular anisotropy and structural disorder. The domain structure corresponding to the major easy axis hysteresis loop has been recorded as a moving visualization of the magnetization reversal process. Using the difference image procedure, individual Barkhausen jumps are observed. Nucleation, annihilation,

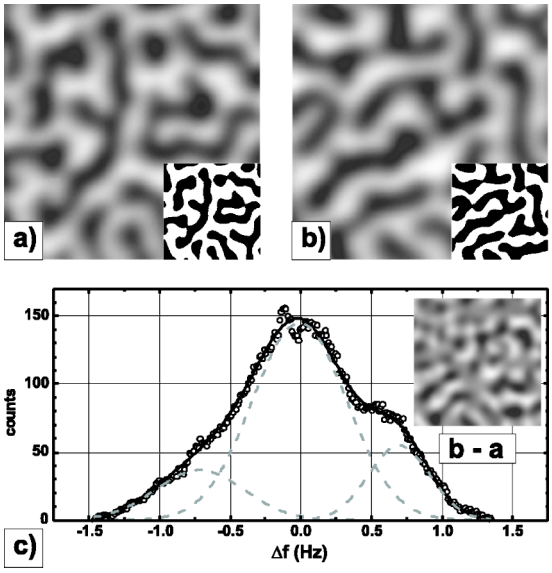

FIG. 10. (a),(b) Remanent domain pattern recorded in the same scan area, with simplified domain patterns as insets. (c) Histogram of the difference image (b)-(a). The solid line is a three peak Gaussian fit representing three possible changes of contrast. The percentage of the image area which has not changed its polarization is higher than expected from a random distribution.

and growth processes could be identified and analyzed in detail. Nucleated and annihilated domains exhibit a Gaussian size distribution whereas growth processes show a critical behavior with an inverse-power law and an exponential cutoff. The distribution of nucleation events can be explained within the critical droplet theory applied to nucleation in an inhomogeneous medium. Calculations concerning the stability of circular domains, i.e., collapse during increasing and elongation during decreasing field, respectively, agree well with the experiment. The distribution of growth processes is discussed in terms of self-organized criticality and domain wall movement in a disordered medium. We conclude that the system cannot be regarded as purely self-organized in a strict sense, because the characteristic structural and magnetic length are of similar magnitude. Secondly, the origin of the exponential cutoff is not a finite size effect, but due to the long-range dipolar interaction. A comparison of domain patterns of different hysteresis loops revealed no correlation with topographic features but highlighted the existence of preferred nucleation sites in a system that contains structural disorder.

ACKNOWLEDGMENTS

We would like to thank U. H. Pi and Z. G. Khim. This work is supported by the Deutsche Forschungsgemeinschaft (Grant No. Wi1277/18-1 and Graduiertenkolleg "Physik nanostrukturierter Festkörper").

*Present address: Yale University, Department of Mechanical Engineering, 15 Prospect Street, New Haven, CT 06511, USA. Email address: marcus.liebmann@yale.edu

†Present address: Department of Materials Science and Engineering, Pohang University of Science and Technology, Pohang, Gyeongbuk 790-784, South Korea.

[1] H. Barkhausen, Z. Phys. Chem., Stoechiom. Verwandtschaftsl. **20**, 401 (1919).

[2] P. J. Cote and L. V. Meisel, Phys. Rev. Lett. **67**, 1334 (1991).

[3] B. Walsh, S. Austvold, and R. Proksch, J. Appl. Phys. **84**, 5709 (1998).

[4] D. H. Kim, S. B. Choe, and S. C. Shin, Phys. Rev. Lett. **90**, 087203 (2003).

[5] A. Schwarz, M. Liebmann, U. Kaiser, R. Wiesendanger, T. W. Noh, and D. W. Kim, Phys. Rev. Lett. **92**, 077206 (2004).

[6] M. Liebmann, U. Kaiser, A. Schwarz, R. Wiesendanger, U. H. Pi, T. W. Noh, Z. G. Khim, and D. W. Kim, J. Magn. Magn. Mater. **280**, 51 (2004).

[7] M. Liebmann, A. Schwarz, S. M. Langkat, and R. Wiesendanger, Rev. Sci. Instrum. **73**, 3508 (2002).

[8] M. Donahue and D. Porter, *Object orientated micromagnetic framework (OOMMF)*, http://math.nist.gov/oommf/

[9] T. R. Albrecht, P. Grütter, D. Horne, and D. Rugar, J. Appl. Phys. **69**, 668 (1991).

[10] A. P. Ramirez, J. Phys. Chem. **9**, 8171 (1997).

[11] J. M. D. Coey, M. Viret, and S. von Molnár, Adv. Phys. **48**, 167 (1999).

[12] Y. Tokura and Y. Tomioka, J. Magn. Magn. Mater. **200**, 1 (1999).

[13] E. Dagotto, T. Hotta, and A. Moreo, Phys. Rep. **344**, 1 (2001).

[14] R. von Helmolt, J. Wecker, B. Holzapfel, L. Schultz, and K. Samwer, Phys. Rev. Lett. **71**, 2331 (1993).

[15] K. Chahara, T. Ohno, M. Kasai, and Y. Kozono, Appl. Phys. Lett. **63**, 1990 (1993).

[16] S. Jin, T. H. Tiefel, M. McCormack, R. A. Fastnacht, R. Ramesh, and L. H. Chen, Science **264**, 413 (1994).

[17] Y. Tokura, A. Urushibara, Y. Moritomo, T. Arima, A. Asamitsu, G. Kido, and N. Furukawa, J. Phys. Soc. Jpn. **63**, 3931 (1994).

[18] M. Ziese, Rep. Prog. Phys. **65**, 143 (2002), and references therein.

[19] H. S. Wang, Q. Li, K. Liu, and C. L. Chien, Appl. Phys. Lett. **74**, 2212 (1999).

[20] D. J. García and B. Alascio, Physica B **320**, 7 (2002).

[21] D. W. Kim, T. W. Noh, H. Tanaka, and T. Kawai, Solid State Commun. **125**, 305 (2003).

[22] C. Kwon, M. C. Robson, J. Y. Gu, S. E. Lofland, S. M. Bhagat, Z. Trajanovic, M. Rajeswari, T. Venkatesan, A. R. Kratz, R. D. Gomez, and R. Ramesh, J. Magn. Magn. Mater. **172**, 229 (1997).

[23] G. van Tendeloo, O. I. Lebedev, and S. Amelinckx, J. Magn. Magn. Mater. **211**, 73 (2000).

[24] J. C. Jiang, E. I. Meletis, and K. I. Gnanasekar, Appl. Phys. Lett. **80**, 4831 (2002).

[25] M. E. Hawley, G. W. Brown, P. C. Yashar, and C. Kwon, J. Cryst. Growth **211**, 86 (2000).

[26] R. Desfeux, S. Bailleul, A. D. Costa, W. Prellier, and A. M. Haghiri-Gosnet, Appl. Phys. Lett. **78**, 3681 (2001).

[27] J. Dho, Y. N. Kim, Y. S. Hwang, J. C. Kim, and N. H. Hur, Appl. Phys. Lett. **82**, 1434 (2003).

[28] R. Desfeux, A. D. Costa, and W. Prellier, Surf. Sci. **497**, 81 (2002).

[29] H. Dulli, P. A. Dowben, S.-H. Liou, and E. W. Plummer, Phys. Rev. B **62**, R14 629 (2000).

[30] Y. Wu, Y. Suzuki, U. Rüdiger, J. Yu, A. D. Kent, T. K. Nath, and C. B. Eom, Appl. Phys. Lett. **75**, 2295 (1999).

[31] A. Hubert and R. Schäfer, *Magnetic domains: The Analysis of Magnetic Microstructures* (Springer-Verlag, Berlin, 1998).

[32] Y. Suzuki, Y. Wu, J. Yu, U. Rüdiger, A. D. Kent, T. K. Nath, and C. B. Eom, J. Appl. Phys. **87**, 6746 (2000).

[33] P. M. Chaikin and T. C. Lubensky, *Principles of Condensed Matter Physics* (Cambridge University Press, Cambridge, UK, 1995).

[34] A. A. Thiele, J. Appl. Phys. **41**, 1139 (1970).

[35] P. Bak, C. Tang, and K. Wiesenfeld, Phys. Rev. Lett. **59**, 381 (1987).

[36] M. R. Freeman and B. C. Choi, Science **294**, 1484 (2001).

[37] L. P. Kadanoff, S. R. Nagel, L. Wu, and S. M. Zhou, Phys. Rev. A **39**, 6524 (1989).

[38] J. P. Sethna, K. A. Dahmen, and C. R. Myers, Nature (London) **410**, 242 (2001).

[39] O. Perkovic, K. Dahmen, and J. P. Sethna, Phys. Rev. Lett. **75**, 4528 (1995).

[40] B. Alessandro, C. Beatrice, G. Bertotti, and A. Montorsi, J. Appl. Phys. **68**, 2901 (1990).

[41] S. Zapperi, P. Cizeau, G. Durin, and H. E. Stanley, Phys. Rev. B **58**, 6353 (1998).

[42] J. M. González, O. A. Chubykalo, and J. González, Phys. Rev. B **55**, 921 (1997).

[43] J. S. Urbach, R. C. Madison, and J. T. Markert, Phys. Rev. Lett. **75**, 276 (1995).